Low Temperature Physics | ARTICLE | scitation.org/journal/ltp

On the possibility of faster detection of magnetic flux changes in a single-photon counter by RF SQUID with MoRe–Si(W)–MoRe junction

Cite as: Fiz. Nizk. Temp. **45**, 906–915 (July 2019); doi: 10.1063/1.5111306
Submitted: 24 May 2019

View Online Export Citation CrossMark

A. P. Shapovalov,[1,4,a)] V. E. Shaternik,[2] O. G. Turutanov,[3,b)] V. Yu. Lyakhno,[3] and V. I. Shnyrkov[4]

AFFILIATIONS

[1]V.N. Bakul Institute for Superhard Materials, National Academy of Sciences of Ukraine, 2 Avtozavodskaya Street, Kiev 04074, Ukraine
[2]G.V. Kurdyumov Institute for Metal Physics, National Academy of Sciences of Ukraine, 36 Academician Vernadsky Boulevard, Kiev 03142, Ukraine
[3]B.I. Verkin Institute for Low Temperature Physics and Engineering, National Academy of Sciences of Ukraine, 47 Nauki Avenue, Kharkov 61103, Ukraine
[4]Kiev Academic University, 36 Academician Vernadsky Boulevard, Kiev 03142, Ukraine

[a)]**Email:** shapovalovap@gmail.com
[b)]**Email:** turutanov@ilt.kharkov.ua

ABSTRACT

The nonhysteretic mode of a RF SQUID with a MoRe–Si(W)–MoRe Josephson junction is analyzed in order to detect the states of a single-photon counter based on a superconducting quantum interferometer with a discrete Hamiltonian. The absorption of a photon with 10 GHz frequency brings the counter to the excited level causing tunnelling into the adjacent potential well and a change in the magnetic flux in the interferometer, which can be detected by the SQUID magnetometer. Measurement of a quantum system requires minimization of the back action of the signal read-out channel at the counter, high sensitivity, and speed of the magnetometer. The MoRe–Si(W)–MoRe contacts are optimized for various concentrations of tungsten (W) in silicon (Si) and barrier layer thickness. It is shown that using MoRe–Si(W)–MoRe contacts with a tungsten concentration of approximately 11% for the RF SQUID at excitation frequencies of ~1 GHz makes it practically an ideal parametric upward frequency shifter with noise determined by the cooled amplifier.

1. INTRODUCTION

At present, considerable experimental and theoretical efforts have been devoted to the studies of single-photon centimeter-range counters ($\lambda \sim 1$–10 cm) based on artificial atoms.[1–7] This interest is primarily stimulated by the possibility of establishing quantum communication channels similar to experiments in the optical range.[8–11] Several types of such counters using different physical principles have been developed for the shortwave range. However, the lowering of microwave photon energy by 4–5 orders of magnitude compared to the quantum of optical radiation ($\lambda \sim 0.3$–3 μm) significantly complicates the actual construction of such a counter, requiring a transition to a new element base and cooling the device down to 10–30 mK.

As for the physical principles, discrete quantum states of Josephson devices can conveniently be used to create an element base of single-photon counters at 2–30 GHz frequencies, since the distances between their energy levels lie in this range. Superconducting "artificial atoms"[1] are considered as such devices—their discrete Hamiltonian has the form $H = \hbar\omega_p\ (n + 1/2)$, where $\hbar = h/2\pi$ is Planck's constant, n is the photon number operator in a nonlinear resonator with its own (plasma) frequency ω_p, which is determined by the Josephson junction itself and the external control parameters.

The structure of a signal read-out channel in the microwave-range photon counter depends on the specific type of superconducting element. For example, the counters based on independent Josephson junctions[2] register junction voltage changes $\Delta V \sim V_c = I_c$

$R_N \sim 1$ mV after the photon is absorbed by the junction due to the transition of the junction with transport current $I \approx 0.95\, I_c$ into a resistive state. Where I_c is the Josephson critical current, and R_N is its normal resistance, taking into account the impedance of a measuring circuit. The speed of such a counter is typically determined by the cooling time of the Josephson junction after it releases the power equivalent $\sim I_c\ V_c$, and not by the bandwidth of the detection scheme. In the temperature range of 10–30 mK, this time reaches several milliseconds.

A very interesting version of a broadband device based on an artificial three-level Λ-atom is considered in Ref. 4. The physical phenomena occurring in a single-photon counter based on an artificial Λ-atom have been analyzed in detail in Refs. 5 and 6. In the scheme for recording the change in the oscillation phase of the parametric generator associated with the Λ-atom, high efficiency and speed (measuring bandwidth $\Delta f \approx 16$ MHz) have been obtained.

Ref. 7 has demonstrated that good speed ($\Delta f \approx 4$ MHz) can be obtained in a single-junction interferometer (RF SQUID) with discrete energy levels and signal read-out channel that uses the nonlinear dependence of the curvature of the qutrit quantum superposition levels on the external magnetic flux. The advantage of using such a circuit for quantum system measurements is the minimum of the measuring circuit back action on the discrete levels of the interferometer (counter). However, further increases in speed of the qutrit-based measuring channel will be limited by the rate at which a superposition state is established, which is related to a slow tunnelling process.

In this article, we will discuss the speed of a single-photon counter with a signal read-out channel based on a classic RF SQUID. The operating principle of such a counter is based on the understanding that after a microwave field quantum is absorbed in the RF SQUID interferometer with a discrete Hamiltonian, the magnetic flux changes by $\Delta\Phi \le \Phi_0/2$ exactly the same as described in Ref. 7, where $\Phi_0 = h/2e$ is a magnetic flux quantum, and e is an electron charge. Measuring a quantum system using a classical device is a non-trivial experimental task and can lead to the degradation of discrete levels of the Josephson oscillator. Let us consider options for reducing the back action of a classic RF SQUID on the quantum system by selecting the excitation frequency and increasing the bandwidth of the measurement circuit while using new Josephson junctions based on the MoRe–Si(W)–MoRe technology.

The magnetic flux change $\Delta\Phi$ in the counter can be measured by a standard DC SQUID whose own energy sensitivity at such low temperatures (∼30 mK) approaches the quantum limit[12,13]

$$\delta\varepsilon = \frac{(\delta\Phi_{\min})}{2L} \ge \frac{\hbar}{2}. \tag{1}$$

Here $\delta\Phi_{\min}$ is the DC SQUID resolution with respect to the magnetic flux in the band of 1 Hz, L is the inductance of the quantization loop. However, the Josephson generation of the DC SQUID at the operating point, and the broadband noise of the shunting resistors can result in an increase of "dark" readings and even in the averaging of the counter's discrete levels.

The back action on the quantum system being measured can be reduced by a magnetometer based on a RF SQUID in a nonhysteretic mode with the parameter $\beta_L = 2\pi L I_c/\Phi_0 < 1$, where I_c is the critical current of the Josephson junction, and L is the geometric inductance of the interferometer. Detailed experimental studies of the RF SQUID characteristics in a nonhysteretic mode have been conducted.[14,15] Due to the absence of phase jumps and associated losses that are typical for the hysteretic mode at $\beta_L > 1$, along with the absence of Josephson generation that is typical for a DC SQUID, the nonhysteretic RF SQUID appears to be an almost ideal parametric upward frequency converter. In general, the bandwidth (speed) and the RF SQUID sensitivity grow with the increase in the pumping frequency ω. However, as the value of ω increases, the "idealistic" conditions of a parametric converter may be impaired due to the Josephson junction properties.

Below, we shall discuss the technology of obtaining MoRe–Si(W)–MoRe junctions and their primary characteristics in terms of RF SQUID operation in a nonhysteretic mode $\beta_L < 1$.[16–18]

2. CHARACTERISTICS OF JOSEPHSON TRANSITIONS OF VARIOUS TYPES

Josephson junctions are usually characterized by three channels of current passage, the relative contribution of each one being determined by the Josephson inductance $L_j = h/2eI_c$, normal resistance R_N, and capacitance C. In this case, the total current passing through the junction is equal to the sum of supercurrent $I_c \sin\varphi$, normal current V/R_N, and displacement current CdV/dt.

For the SQUID analysis, it is appropriate to consider frequencies corresponding to these parameters.[19] The first one—plasma frequency of the junction—is defined as

$$\omega_p = \frac{1}{\sqrt{L_j C}} = \sqrt{\frac{2eI_c}{\hbar C}} \sim \left(\frac{j_c}{c}\right)^{1/2}, \tag{2}$$

where $j_c = I_c/S$ is the critical current density, S is the area of the junction, and here $c = C/S$ is the specific capacitance. The second one is the characteristic frequency of the junction

$$\omega_c = \frac{R_N}{L_j} = \frac{2\pi V_c}{\Phi_0}, \tag{3}$$

which is proportional to the important characteristic of the junction $V_c = I_c\ R_N$ and determines the frequency boundary of the non-stationary Josephson effect. The third frequency is determined by the time RC of the equivalent junction loop and is almost independent of its area

$$\omega_{RC} = \frac{1}{R_N C} = \frac{\omega_p^2}{\omega_c}. \tag{4}$$

The dynamics of the junction at frequencies up to ω_c can be conveniently analyzed using the dimensionless parameter β_c, which characterizes the attenuation in the system:

$$\beta_c = \frac{2\pi R_N^2 I_c C}{\Phi_0}. \tag{5}$$

Contemporary superconductor-insulator-superconductor (SIS) Josephson tunnel junctions are manufactured[20] using superconducting niobium films separated by a thin dielectric barrier made of aluminium oxide. Junctions Nb–Al–Al_2O_3–Nb have good reproducibility, resistance to thermocycling, and a wide range of critical current densities $j_c = 0.3–45\ \mu A/\mu m^2$. The high specific capacitance of such junctions $c \approx 40–60\ fF/\mu m^2$ reduces the values of plasma frequency ω_p and increases the junction quality $\sim(\beta_c)^{1/2}$, resulting in $\beta_c \gg 1$. In order to satisfy the requirement that $\beta_c < 1$, which is necessary for SQUID operation, the SIS junctions are shunted via an additional thin film resistor. In the SNS (superconductor–normal metal–superconductor) thin film junctions, the condition $\beta_c < 1$ is automatically fulfilled due to the small values of normal resistance and specific capacitance. However, it is precisely the low resistance of SNS junctions that limits their use in most practical devices, including SQUIDs. Attempts to reduce the influence of proximity effect and to increase normal resistance by creating multilayer structures with additional dielectric barriers such as superconductor–insulator–normal metal–insulator–superconductor (SINIS) have not yet resulted in obtaining better parameters than in SIS junctions.[20] The ScS (superconductor–constriction–superconductor) point contacts[19] have a low capacitance, high values of plasma frequency ω_p and characteristic frequency ω_c. Thus, they can be used in unique physical experiments requiring junctions with ultimate parameters. In this regard, atomic-size contacts are a very good example of the wide "universality" of ScS junctions.[21] However, instability and non-resistance to thermocycling of the ScS contacts make their practical use significantly limited.

Even though SIS junctions are prevailing in practical devices, attempts have been recently renewed[22–27] to improve the characteristics defined by Formulas (2)–(5) by creating structures with direct conductivity. The central technological idea is well known and involves the creation of weak link using a normal metal with conductivity σ_n which is small compared with the standard conductivity of superconducting banks σ_s. In practice, in order to reduce the degradation of the superconducting order parameter in the banks due to the proximity effect, a more stringent condition must be met,[28] i.e., $\sigma_s / \xi_s \gg \sigma_n/\xi_n$, where ξ_s and ξ_n are coherence lengths in superconducting and normal metals, respectively. Moreover, in order to obtain large values of normal contact resistance, and thus to enhance important contact characteristics ω_c and V_c, the characteristic size of the normal weak link must be small: $a \approx \xi_n$. These conditions can be met in film structures MoRe–Si(W)–MoRe.

3. PRODUCTION AND EXPERIMENTAL PARAMETERS OF TRANSITIONS IN MORE–SI(W)–MORE

A vacuum universal post VUP-5 M (made by SELMI, Sumy, Ukraine) was used to implement the production processes for manufacturing superconducting films and heterostructures based on them. The use of 5P4E polyphenyl ether (with characteristics similar to Convalex 10, Agilent, USA) as a working fluid in the diffusion pump allowed us to obtain vacuum in the VUP-5 M chamber at 2×10^{-5} Pa. In order to form three-layer MoRe–Si(W)–MoRe film structures,[16–18] we used magnetron sputtering of MoRe and Si(W) targets in argon flow (under pressure $P \sim 0.1$ Pa)

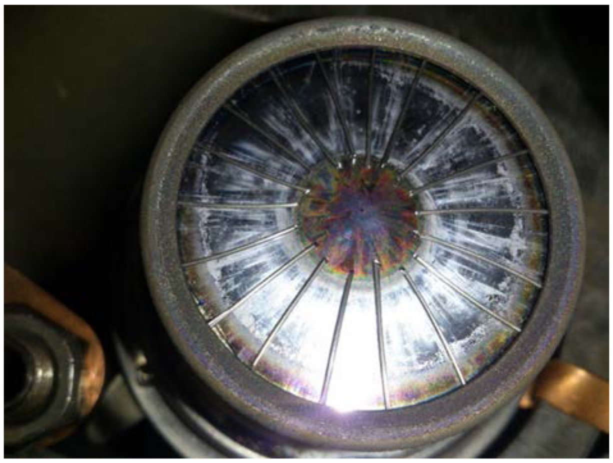

FIG. 1. A photo of the composite Si + W target for the deposition of the barrier layer. Tungsten wires are located on the silicon plate.

followed by deposition of thin MoRe and Si(W) films on polished polycrystalline substrates Al_2O_3 (polycor). A set of three metallic shadow masks was used to form a planar transition topology. The successive deposition of each layer of the MoRe–Si(W)–MoRe structure occurred with opening the chamber in order to move a sample between different mask positions.

The MoRe target was made of 0.5 mm foil consisting of molybdenum (52 at% Mo) rhenium (48 at% Re) alloy. The composite target (Si + W) for obtaining Si(W) films (Fig. 1) was produced from a monocrystalline silicon plate (purity 99.99 at%) and was soldered with indium to the magnetron surface to cool it down to room temperature during sputtering. Ten to twelve 0.3 mm tungsten (W) wires about 10 mm long were placed on the target's surface. The wires were located in the erosion zone of the Si target perpendicular to the erosion ring and crossing it. During magnetron sputtering of this composite target, the W wires were heated up to a temperature of no more than 700°C, as evidenced by dark red glow.

During simultaneous deposition from the composite target (Si + W), tungsten clusters are formed in the Si(W) hybrid barrier by self-organization. The results of electron microscopic studies of the microstructure of Si(W) model barrier layers (~100 nm thick) on KCl substrates indicate that tungsten is self-organized into nanoclusters (see Fig. 2) inside the barrier. In the Si(W) barrier layers being studied, tungsten agglomerated into clusters of a characteristic size that was approximately the same as the barrier thickness. As the structural analysis has shown, both silicon and tungsten are in an amorphous state when the Si(W) barrier is produced by such technology.

Based on the data obtained from electron microscopic studies, a simple model can be suggested for the possible arrangement of W nanoclusters in Si(W) hybrid barriers (Fig. 3) depending on the amount of tungsten contained in them.

The proposed barrier model is confirmed by the results of atomic force microscopy (AFM) of the Si(W) films presented in

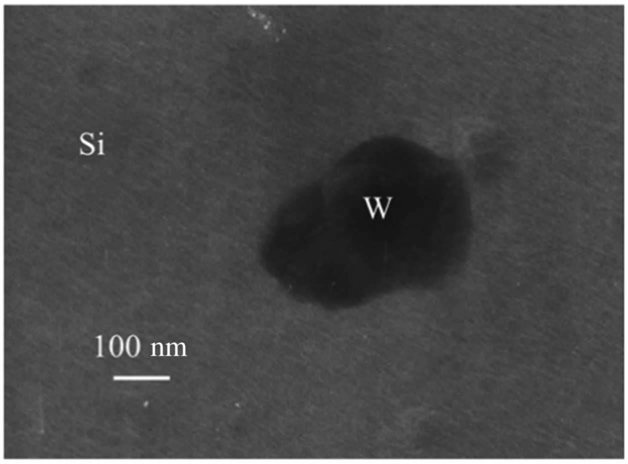

FIG. 2. Image of the Si(W) model barrier layer (100 nm) obtained by transmission electron microscopy using a JEOL JEM-2000FX microscope.

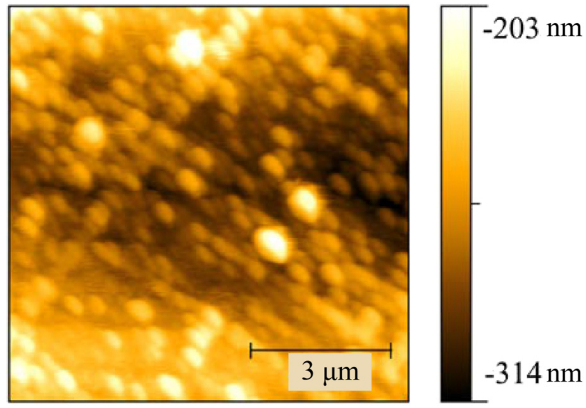

FIG. 4. Image of the Si(W) film relief obtained using AFM in the non-contact mode. The substrate is polycor (Al_2O_3).

Fig. 4. In the non-contact oscillating mode, AFM measures the phase-sensitive contrast of the hybrid barrier layer surface and provides quantitative data only on the distances between clusters. It is well known that the gradients of the van der Waals forces in the vertical direction for the metallic phase of tungsten and the semiconductor matrix are significantly different, therefore the AFM measures "imaginary relief" (images of clusters in the matrix), which provides information regarding the location of tungsten clusters in the Si matrix.

We have experimentally studied the current-voltage characteritics (I–V curves) of the produced MoRe–Si(W)–MoRe heterostructures (one of such characteristics is shown in Fig. 5 for the heterostructure with a 15 nm barrier thickness and 10% tungsten content). In order to obtain an average value of the characteristic voltage V_c of the heterostructures, I-V measurements of heterostructures having a large (100 × 100 μm) area were carried out. We have studied how the value of the superconducting critical current I_c in the created heterostructures MoRe–Si(W)–MoRe depends on temperature T. The typical experimental dependence I_c (T) of the heterostructure containing tungsten in the barrier Si(W) ~ 10 at%, and theoretical curves for various theoretical models are shown in Fig. 6.

This dependence is similar to the experimental dependence I_c (T)[22] which was obtained while studying Nb/α–Si/Nb heterostructures (where α–Si is an amorphous silicon doped by tungsten (W) to the level of 8–10 at%), in which resonant-percolation charge transport was realized in the barrier.[18] At the same time, as seen in Fig. 6, the dependence I_c (T) obtained here is also similar to the

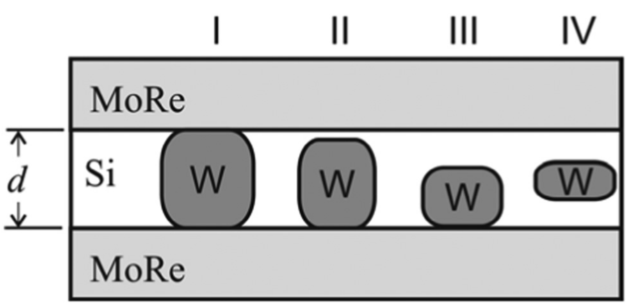

FIG. 3. A model of the Si(W) barrier layer contained between superconductive films MoRe. The thickness of the silicon (Si) layer, doped with tungsten nanoclusters (W), is marked by letter *d*. Various possible sizes and locations of tungsten nanoclusters within the barrier layer that depend on the tungsten concentration and the vacuum deposition regime of the barrier layer, are denoted by Roman numerals.

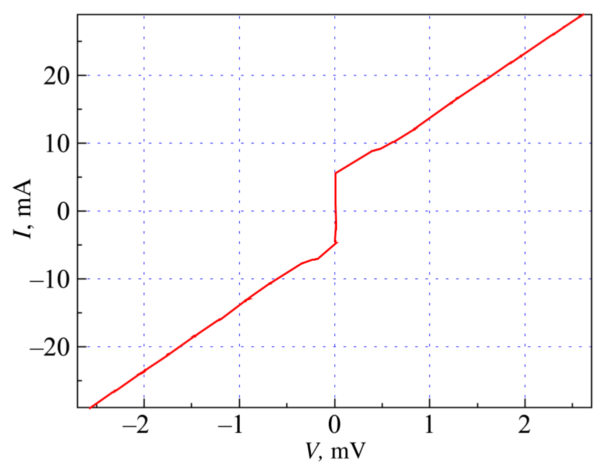

FIG. 5. Typical I-V curves for the MoRe/Si(W)/MoRe junctions with an area of 100 × 100 μm with the tungsten content in the barriers $n_W \approx 10$ at% at the temperature of 4.2 K. The thickness of barrier layers Si(W) $d = 15$ nm, the critical current $I_c = 0.5$ mA, dynamic resistance $dV/dI|_{6\ \mathrm{mV}} = 0.11$ Ohm, characteristic voltage $I_C R_N = 0.53$ mV.

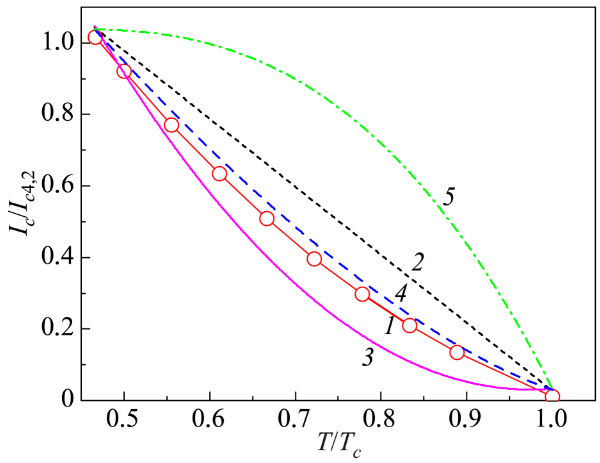

FIG. 6. Typical experimental dependence of the critical current on the temperature I_c of the heterostructure being studied (*1*). A few theoretical dependences[24,29] are shown for comparison, namely, a junction model with resonant tunnelling through a localized state (*2*), a SINIS double-barrier junction (*3*), a whisker junction model (*4*), and a SIS junction model (*5*).

dependence obtained for a superconducting whisker model.[29] What is common to these types of dependences is the quasi-one-dimensional nature of the charge transport.

For junctions MoRe/Si(W)/MoRe, the values of characteristic frequencies ω_c, ω_p, ω_{RC} , specific capacitance c and resistances R_N are in good agreement with the results obtained in Ref. 24 for contacts Nb/Si(W)/Nb. However, we believe that replacing a very active getter Nb by MoRe in a planar film junction will increase the long-term stability of the Josephson junction and of the signal read-out channel based on the RF SQUID. Preliminary experiments have shown that the critical current of described heterostructure did not change after three-month storage at room temperature.

4. RF SQUID WITH MoRe–Si(W)–MoRe CONTACT FOR A SINGLE PHOTON READ-OUT CHANNEL

The principle of detecting resonant single microwave photons with the same frequency as the frequency of transition between the ground E_0 and excited E_1 states, $f = (E_1–E_0)/h$ in an artificial atom with double-well potential is schematically shown in Fig. 7(a). To implement further assessment of specific values of the numerical parameters, we shall assume that $f = 10$ GHz, which is a typical value for superconducting qubits considered as "artificial atoms".[7] In its initial state, the system is in the ground state E_0 in the left well. After absorbing the resonance photon, it transits to the excited state E_1 and tunnels into the right well. The tunnelling decay rates Γ_1 and Γ_0 of the metastable states from levels E_1 and E_0 depend exponentially on the barrier's width and height and may differ by three orders of magnitude,[30] which is schematically shown by arrows of different lengths. When the system transits to the right well, the average value of magnetic flux changes to $\Delta\Phi \leq \Phi_0/2$ (in this particular case $\Delta\Phi \approx 0.3\,\Phi_0$), and this signal is registered by a SQUID magnetometer.

A portion of the high-frequency power of the RF SQUID pump generator will get into the counter through inductive coupling and may lead to "dark" counts due to the multi-photon transitions between the levels.[31,32] To suppress this effect, we shall select the pumping frequency from the condition $\omega/2\pi \leq f/10$ such that its value is between the peaks of multi-photon resonances [Fig. 7(b), shown by an arrow]. Lowering the pumping frequency below 0.5 GHz is not reasonable due to the proportional deterioration of the sensitivity and the parametric converter bandwidth. For the same purpose, we shall consider only the limit of small amplitudes of the RF SQUID excitation.

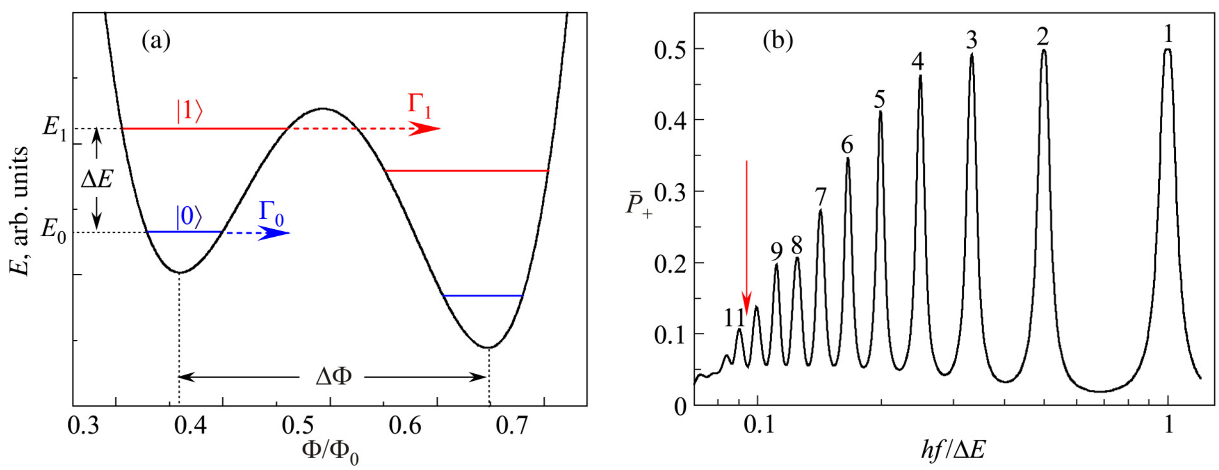

FIG. 7. Changes in the average value of magnetic flux $\Delta\Phi$ in the counter, induced by a photon with energy ΔE (a). The probability of multi-photon absorptions in a two-level nonlinear artificial atom (based on Fig. 5 from publication.[31]) The numerals above the peaks of absorption probability indicate the number of photons absorbed in one action. The optimal RF SQUID excitation frequency is shown by the arrow (b).

In order to analyze the dynamics of a magnetometer based on a RF SQUID with $\beta_L < 1$, it is important to select an adequate model of its primary element, the Josephson junction. Experimental studies[18,24] show that at small (∼11%) concentrations of tungsten in the Si(W) barrier, most junction properties at low voltages are described by a simple resistive model with good accuracy. This fact simplifies the analysis of the signal and noise characteristics of the nonhysteretic mode of RF SQUID operation, making it possible to use classical analysis even for high-frequency signals and pumping.

The basic magnetometer circuit for the selected pumping frequency range is presented in Fig. 8(a). The RF SQUID interferometer with $\beta_L < 1$ is inductively coupled to the oscillatory circuit (tank) having a resonance frequency $\omega_T = (L_T \times C_T)^{-1/2}$, where L_T and C_T are the inductance and capacitance of the oscillatory circuit, respectively. The current in the circuit at the frequency of $\omega \approx \omega_T$ is set by the pump generator. The nonlinearity of the Josephson junction determines interferometer's impedance, which is brought into the resonant circuit due to the inductive coupling. In such a system, the inverse effective quality factor 2δ, and effective resonant frequency mismatch of the circuit 2ξ, depend on the changes of the external flux $\varphi_e = 2\pi\Phi_e/\Phi_0$ and amplitude a of oscillations in the circuit.

In the limit of small values of the SQUID primary parameter $\beta_L \ll 1$, taking into account nonadiabatic effects proportional to $q = \omega L/R$, the expressions for these values[33] have the following form

$$2\delta(a, \varphi_e) = Q^{-1} + \frac{k^2}{(1+q^2)}\left[q - \beta_L \frac{2J_1(z)}{z}\left(\frac{2q}{1+q^2}\right)\cos\varphi_e\right], \quad (6a)$$

$$2\xi(a, \varphi_e) = 2\xi_0 - \frac{k^2}{(1+q^2)}\left[q^2 + \beta_L \frac{2J_1(z)}{z}\left(\frac{1-q^2}{1+q^2}\right)\cos\varphi_e\right]. \quad (6b)$$

Here Q is the quality factor of an unloaded resonant circuit, $k = M\,(LL_T)^{-1/2}$ is the coupling coefficient between the interferometer and resonant circuit, J_1 (z) is the first-order Bessel function from argument $z = a/(1+q^2)^{1/2}$, $\xi_0 = (\omega - \omega_T)/\omega_T \ll 1$ is generator frequency mismatch from the circuit resonant frequency ω_T. The expression for 2δ (a, φ_e) and 2ξ (a, φ_e), taking into account the terms proportional to β_L^2, have been obtained in Ref. 14. According to Ref. 14, when the junction's critical current increases to make the $\beta_L^2 \approx 0.5$–0.6, the main results that follow from Eqs. (6a), (6b), remain qualitatively valid. At large values of $q \sim 1$, the losses in the interferometer significantly increase, the modulation depth of the tank characteristics by the signal magnetic flux φ_e rapidly decreases, and the RF SQUID interferometer's performance deviates from the "ideal."

We shall consider nano-sized (10–50 nm) clusters of tungsten in the MoRe–Si(W)–MoRe contacts as a shunt built into the contact and having sufficiently high resistance R compared to "traditional" materials used in SNS junctions (see Fig. 3). Let us assess parameter q, assuming that the geometric inductance of the interferometer is $L \approx 0.1$ nH. As shown in experimental studies,[18,22–24] when the barrier thickness is $d \approx 15$–20 nm and tungsten concentrations are ∼11%, the MoRe–Si(W)–MoRe junctions and their predecessors Nb–a–Si–Nb are characterized by high current density $j_c \approx 5$–$55\ \mu A/\mu m^2$, specific resistance $r \approx 20$–$25\ Ohm/\mu m^2$ and capacitance $c \approx 5\ fF/\mu m^2$. For a junction with an area of $S = 0.5\ \mu m^2$, the critical current $I_c = j_c S$ provides the value of SQUID primary parameter $\beta_L \approx 1$ at resistance $R_N = rS \approx 40$–50 Ohm, which leads to $q \leq 0.015$ for the excitation frequency 1 GHz.

The absence of electrodynamic hysteresis on the I-V curves of autonomous junctions, as well as RF and DC SQUIDs, requires large attenuation, i.e. the values of $\beta_c < 1$. The low specific capacitance of MoRe–Si(W)–MoRe junctions makes it possible to fulfil this requirement. For example, for the above junction with the area $S = 0.5\ \mu m^2$, $I_c \approx 2.75\ \mu A$, $R_N \approx 40$–50 Ohm, we obtain that $\beta_c \leq 0.13$.

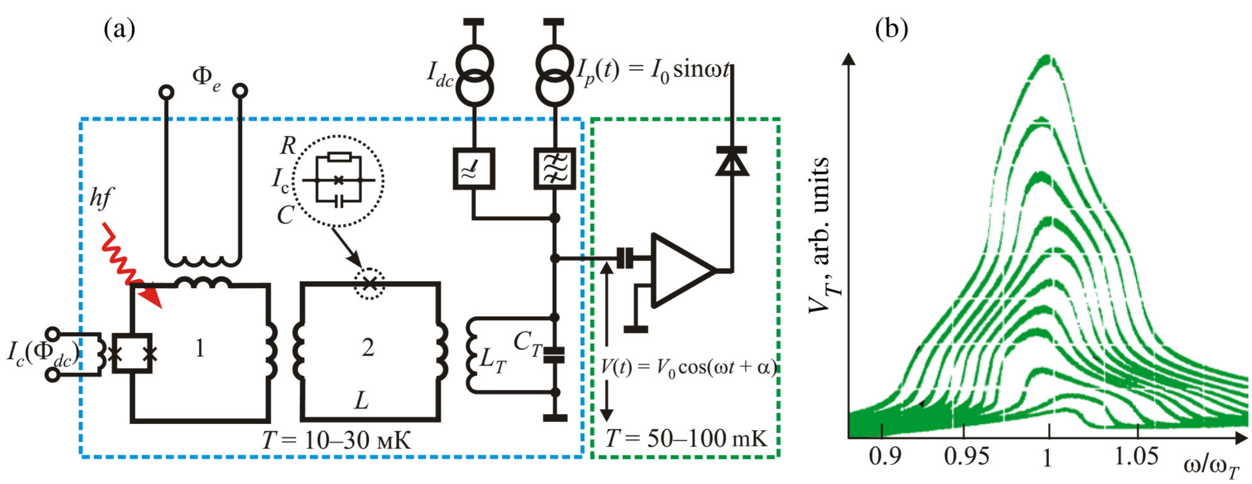

FIG. 8. The RF SQUID circuit with the preamplifier being cooled down to $T \approx 50$ mK for the read-out channel of changes to the magnetic flux in a single-photon counter (a). A set of the RF SQUID amplitude-frequency characteristics in a nonhysteretic mode for various amplitudes of RF-excitation current in the SQUID (b).

Taking into account the contribution of an additional (parasitic) capacitance C_S, we used here the value of total capacitance as $C = C_J + C_S \approx 6$ fF.

Even though the physical processes in the MoRe–Si(W)–MoRe junctions have not yet been analyzed in full, an important practical conclusion can already be made based on the published results.[16–18,22–27] The low values of intrinsic capacitance and the rather high values of resistance in the MoRe–Si(W)–MoRe junctions allow us to consider the RF SQUID in a nonhysteretic mode as an ideal parametric converter. When the RF SQUID is analyzed at the excitation frequencies $\omega/2\pi \approx 1$ GHz, the assumption can be made that $q \approx 0$, i.e., it is possible to limit the consideration to the case when the primary dependence of the interferometer $\varphi[\varphi_e(t)]$ almost coincides with the stationary dependence. In this limit, the resonant frequency ω_R of a nonlinear circuit as a function of external flux φ_e and oscillation amplitude a, taking into account the terms proportional to β_L^2, has the form[14]

$$\omega_R(a, \varphi_e) = \omega_T\left[1 + k^2\beta_L\frac{J_1(a)}{a}\cos\varphi_e - \frac{1}{2}k^2\beta_L^2\frac{J_1(2a)}{2a}\cos 2\varphi_e\right]. \quad (7)$$

In the mode $\beta_L < 1$, $k^2Q\beta_L \le 1$ all RF SQUID conversion coefficients (with respect to the phase $\eta_\Theta \sim \partial\Theta/\partial\varphi_e$, frequency $\eta_\omega \sim \partial\omega_R/\partial\varphi_e$, and amplitude $\eta_a \sim \partial a/\partial\varphi_e$) increase proportional to β_L. At $\beta_L \cong 1$, their effective values reach $\eta_0 = (\omega/k)(L_T/L)^{1/2}$, which, taking into account excitation frequency $\omega/2\pi \approx 1$ GHz, bandwidth $\Delta\omega/2\pi \ge 10$ MHz, $k^2Q \approx 1$, gives $\eta_0 \approx 4 \times 10^{11}$ V/Wb.

When estimating the sensitivity of the RF SQUID in a nonhysteretic mode, the noise of an interferometer with a MoRe–Si(W)–MoRe junction can be neglected due to low operating temperature $T \approx 30$ mK, interferometer's short time L/R and sufficiently large values of $V_c = I_cR \approx 100\,\mu$V. Practically, the magnetic flux resolution of the RF SQUID with the conversion coefficient $\eta_0 \approx 4 \times 10^{11}$ V/Wb will be limited by the amplifier and resonant circuit, the noise temperature of which can be presented as follows (taking into account the fluctuation effect of the first stage of an RF amplifier)

$$T_T = T_{T0} + \frac{QL_T\omega_T}{R_a}T_a, \quad (8)$$

where T_{T0} is the circuit's physical temperature, T_a and R_a are the amplifier's temperature and its input resistance. The temperature value T_{T0} can be reduced by placing the amplifier's first stage in the refrigerator zone with temperature $T \approx 50$–100 mK. Assuming that a two-stage amplifier with low power consumption of direct current $P_{dc} \approx 7$–$10\,\mu$W[34] is placed at $T \approx 50$ mK, the estimation of the magnetometer's sensitivity to magnetic flux results in $\delta\Phi_{min} \approx 5 \times 10^{-7}\,\Phi_0$ Hz$^{-1/2}$. For the magnetometer's intrinsic energy sensitivity [Eq. (1)], we obtain $\delta\varepsilon \approx 5\times10^{-33}$ J/Hz, which is significantly higher than the quantum limit and justifies the use of a resistive model to describe an interferometer with a Josephson junction. Assuming that, after the absorption of a quantum of the electromagnetic field, the change in the magnetic flux in the detector $\Delta\Phi \approx 0.3\,\Phi_0$, and the transformation ratio of the magnetic flux from the detector to the magnetometer 1/300, we obtain a signal/noise ratio ≈ 1 for the 10 MHz magnetometer band. In order to confidently measure the flux with a signal/noise ratio ≈ 3 while preserving the frequency band, it is possible to increase the coupling factor up to 0.01, though this will increase the undesirable back action on the detector. Subsequent studies of low power operational amplifiers[35,36] for a frequency range of 0.5–1 GHz have shown that its stages can even be located at 15–20 mK.

As shown in publications,[15,37,38] the RF SQUID conversion coefficient η at small excitation amplitudes can be increased by an order of magnitude and more when the condition $k^2Q\beta_L > 1$, $\beta_L < 1$ is satisfied [see Fig. 8(b)]. This reduces the contribution of the amplifier noises to the overall noise of the magnetometer, increasing its sensitivity. This effect is characteristic of parametric modulator-demodulator-type amplifiers such as the RF SQUID in the mode of $\beta_L < 1$ with the MoRe–Si(W)–MoRe junction. However, it should be noted that in this case the maximum frequency of the measured signal (speed) will decrease proportionally to the increase of the conversion coefficient $\sim (\omega/2\pi Q)(\eta_0/\eta)$.

Moreover, when the conversion coefficient increases, the inverse fluctuation effect of the RF SQUID on the measured quantum object significantly increases (proportionally to η/η_0), which may lead to the averaging of the photons' discrete levels in the detector.

5. DISCUSSION OF RESULTS

When creating a broadband signal read-out channel in a single-photon detector based on a RF SQUID, the most important advantage of planar thin film MoRe–Si(W)–MoRe junctions, as compared with SIS tunnel structures, is a low value of their specific capacitance. This is due to the fact that the thickness of the Si(W) barrier layer with tungsten concentrations of 10–11% may be $d \approx 20$–30 nm at the critical current densities which are comparable or even greater than in the SIS tunnel junctions.[18,24] Note that a significant decrease of the displacement current in the MoRe–Si(W)–MoRe junctions improves the dynamics of both RF and DC SQUIDs for any applications. At such barrier thicknesses, the values of the junctions' characteristic voltages V_c are within the range of 100–200 μV. As follows from the theory for the SNS structures,[28] any further increase in the thickness of the Si(W) barrier layer will lead to a rapid decrease of $V_c \approx \frac{2\Delta}{e}\exp\left(-\frac{d}{\xi_W}\right)$, where Δ is the energy gap in the MoRe "banks," and ξ_W is coherence length in tungsten.

Another significant advantage is that the MoRe–Si(W)–MoRe junction is a "self-shunted" structure which does not require manufacturing of an external shunt in order for the condition $\beta_c < 1$ to be fulfilled; for small area junctions (1 × 1 μm), the resistance of the barrier layer is in the interval of 10–40 Ohm. The wide spread of values V_c and R_N in the MoRe–Si(W)–MoRe junctions is not a critical disadvantage for a RF SQUID with the excitation frequency of 1 GHz, because it is always possible to select the critical current required to fulfil the conditions $\beta_c < 1$, $\beta_L \cong 1$.

Nevertheless, the technology of junction production needs to be improved and requires further research. In particular, what is needed is the creation of MoRe–Si(W)–MoRe Josephson junctions with characteristics close to the characteristics of Nb–Si(W)–Nb[22–24] or high impedance ScS junctions (which implies an increase of characteristic voltage V_c, and thus an expansion of the frequency range in which they can be applied). In particular, this will increase the sensitivity and will speed up the single-photon counter. Then, in the described two-level system with $f = (E_1 - E_0)/h \cong 10$ GHz, the excitation frequency of the RF SQUID can be raised, and, consequently, so can the conversion coefficient, bandwidth, and sensitivity. In this case, the pumping frequency should be chosen above the system absorption spectrum ($\omega/2\pi > f$), such as 20 GHz, for example. It should be noted that in the above analysis of the RF SQUID operations at the frequency of 1 GHz, the device was considered as an almost ideal parametric converter ($q \sim 0.01$), which has a very small back action on the quantum system being measured (photon counter). At higher frequencies, it ceases to be "ideal." However, even at the pumping frequency of about 20 GHz, the nonadiabaticity parameter for a SQUID with a MoRe–Si(W)–MoRe junction may remain substantially less than one ($q \leq 0.3$), which, as the analysis shows,[39] still does not lead to significant sensitivity degradation of the parametric converter. But then, the read-out channel bandwidth in the single-photon counter can be significantly increased (almost proportionally to the pumping frequency ratio), and the range 50–100 MHz does not seem unrealistic.

6. CONCLUSIONS

When creating broadband receivers based on high sensitivity SQUIDs, MoRe–Si(W)–MoRe Josephson planar junctions have obvious advantages over traditional SIS niobium tunnel junctions with an oxide barrier layer 1.5–2 nm thick.

A relatively small displacement current plays an important role in the dynamics of the RF SQUIDs. This implies low capacitance C of the MoRe–Si(W)–MoRe junctions which can be calculated by a usual formula $C = \varepsilon_0 \varepsilon_b S/d$, where $\varepsilon_0 \approx 8.85 \times 10^{-12}$ F/m, ε_b is the relative dielectric permittivity of the barrier layer, and S is the junction area. Since d in such junction could be 30 nm, the characteristic value C is significantly less than in SIS junctions, which have the values of $\beta_c \geq 10^2$.

In order to increase attenuation and fulfil the condition $\beta_c < 1$, tunnel SIS junctions must be shunted by additional external resistance $R \approx 2$ Ohm. In the considered self-shunted MoRe–Si(W)–MoRe junctions, this role is performed by a tungsten nanocluster with a resistance $R \geq 10$ Ohm located in the matrix of doped amorphous silicon.

The characteristics of the MoRe–Si(W)–MoRe planar junctions make it possible to increase the sensitivity and speed of the signal read-out channel in the single-photon counter in the centimeter wavelength range, which is a high-priority objective in quantum measurement technique.

Let us finally note that, compared with traditional niobium (Nb) films, the physical and chemical properties of the MoRe films result in a high stability of their characteristics over time, and simplify the production and lithography processes of the MoRe–Si(W)–MoRe junctions.

The current developments in Josephson junction technologies are typically aimed at optimizing their parameters to create specific devices.[40,41]

In this sense, we hope that the improvement of the technological process for obtaining small area MoRe–Si(W)–MoRe junctions will contribute to the creation of almost ideal parametric amplifiers based on SQUIDs in a nonhysteretic mode with pumping frequencies ~ 20 GHz and a bandwidth of 50–100 MHz.

ACKNOWLEDGMENTS

The authors wish to thank A. A. Kordyuk and S. N. Shevchenko for the stimulating discussion of the results and prospects of further work.

REFERENCES

[1] X. Gu, A. F. Kockum, A. Miranowicz, Y.-X. Liu, F. Nori, arXiv:1707.02046 [quant-ph] (2017).
[2] Y.-F. Chen, D. Hover, S. Sendelbach, L. Maurer, S. T. Merkel, E. J. Pritchett, F. K. Wilhelm, and R. McDermott, Phys. Rev. Lett. **107**, 217401 (2011).
[3] I.-C. Hoi, C. M. Wilson, G. Johansson, T. Palomaki, B. Peropadre, and P. Delsing, Phys. Rev. Lett. **107**, 073601 (2011).
[4] K. Inomata, Z. Lin, K. Koshino, W. D. Oliver, J.-S. Tsai, T. Yamamoto, and Y. Nakamura, Nat. Commun. **7**, 12303 (2016).
[5] K. Koshino, Z. Lin, K. Inomata, T. Yamamoto, and Y. Nakamura, Phys. Rev. A **93**, 023824 (2016).
[6] K. Koshino, K. Inomata, Z. Lin, Y. Nakamura, and T. Yamamoto, Phys. Rev. A **91**, 043805 (2015).
[7] V. I. Shnyrkov, W. Yangcao, A. A. Soroka, and O. G. Turutanov, V. Y. Lyakhno, Fiz. Nizk. Temp. **44**, 281 (2018) [Low Temp. Phys. **44**, 213 (2018)].
[8] G. N. Gol'tsman, O. Okunev, G. Chulkova, A. Lipatov, A. Semenov, K. Smirnov, B. Voronov, A. Dzardanov, C. Williams, and R. Sobolewski, Appl. Phys. Lett. **79**, 705 (2001).
[9] R. H. Hadfield, Nat. Photon. **3**, 696 (2009).
[10] D. Roy, C. M. Wilson, and O. Firstenberg, Rev. Mod. Phys. **89**, 021001 (2017).
[11] Y. P. Korneeva, M. Y. Mikhailov, Y. P. Pershin, N. N. Manova, A. V. Divochiy, Y. B. Vakhtomin, A. A. Korneev, K. V. Smirnov, A. G. Sivakov, and A. Y. Devizenko, Supercond. Sci. Technol. **27**, 095012 (2014).
[12] M. B. Ketchen, IEEE Trans. Magn. MAG **17**, 387 (1981).
[13] C. D. Tesche and J. Clarket, J. Low Temp. Phys. **37**, 397 (1979).
[14] V. I. Shnyrkov, V. A. Khlus, and G. M. Tsoi, J. Low Temp. Phys. **39**, 477 (1980).
[15] I. M. Dmitrenko, G. M. Tsoi, V. I. Shnyrkov, and V. V. Kartsovnik, J. Low Temp. Phys. **49**, 417 (1982).
[16] V. Lacquaniti, C. Cassiago, N. De Leo, M. Fretto, A. Sosso, P. Febvre, V. Shaternik, A. Shapovalov, O. Suvorov, M. Belogolovskii, and P. Seidel, IEEE Trans. Appl. Supercond. **26**, 1100505 (2016).
[17] V. E. Shaternik, A. P. Shapovalov, and T. A. Prikhna, O. Y. Suvorov, M. A. Skorik, V. I. Bondarchuk, and V. E. Moshchil, IEEE Trans. Appl. Supercond. **27**, 1800507 (2017).
[18] V. E. Shaternik and A. P. Shapovalov, A.Y. Suvorov, Fiz. Nizk. Temp. **43**, 1094 (2017) [Low Temp. Phys. **43**, 877 (2017)].
[19] K. K. Likharev, Rev. Mod. Phys. **51**, 101 (1979).
[20] *Niobium Integrated Circuit Fabrication, Process #03-10-45, Design rules, Revision #25* (Hypres, Inc., 2012).
[21] N. Agrait, A. L. Yeyati, and J. M. van Ruitenbeek, Phys. Rep. **377**, 81 (2003).
[22] A. L. Gudkov, M. Y. Kupriyanov, K. K. Likharev, JETP **94**, 319 (1988) [Sov. Phys. JETP **68**, 1478 (1988)].
[23] V. A. Kulikov, L. V. Matveets, A. L. Gudkov, V. N. Laptev, and V. I. Makhov, IEEE Trans. Magn. MAG **27**, 2468 (1991).
[24] A. L. Gudkov, M. Y. Kupriyanov, A. N. Samus, JETP **141**, 939 (2012) [JETP **114**, 818 (2012)].
[25] B. Baek, P. D. Dresselhaus, and S. P. Benz, Phys. Rev. B **75**, 054514 (2007).

[26]D. Olaya, P. D. Dresselhaus, S. P. Benz, A. Herr, Q. P. Herr, A. G. Ioannidis, D. L. Miller, and A. W. Kleinsasser, Appl. Phys. Lett. **96**, 213510 (2010).
[27]D. Olaya, P. D. Dresselhaus, and S. P. Benz, IEICE Trans. Electron. **E93-C**, 463 (2010).
[28]Z. G. Ivanov, M. Y. Kupriyanov, K. K. Likharev, S. V. Meriakri, O. V. Snigirev, Fiz. Nizk. Temp. **7**, 560 (1981) [Sov. J. Low Temp. Phys. **7**, 274 (1981)].
[29]V. M. Dmitriev, I. V. Zolochevsky, T. V. Salenkova, and E. V. Khristenko, Fiz. Nizk. Temp. **31**, 169 (2005) [Low Temp. Phys. **31**, 127 (2005)].
[30]D. A. Bennett, L. Longobardi, V. Patel, W. Chen, D. V. Averin, and J. E. Lukens, Quantum Inf. Proc. **8**, 217 (2009).
[31]S. N. Shevchenko, A. S. Kiyko, A. N. Omelyanchouk, and W. Krech, Fiz. Nizk. Temp. **31**, 752 (2005) [Low Temp. Phys. **31**, 569 (2005)].
[32]S. N. Shevchenko, A. N. Omelyanchouk, and E. Il'ichev, Fiz. Nizk. Temp. **38**, 360 (2012) [Low Temp. Phys. **38**, 283 (2012)].
[33]V. V. Danilov and K. K. Likharev, Radiotekhnika i Elektronika **25**, 1725 (1980) [Radio Engineering and Electronic Physics **25**, 112 (1980)].
[34]A. M. Korolev, V. M. Shulga, and V. I. Shnyrkov, Rev. Sci. Instrum. **82**, 016101 (2011).
[35]A. M. Korolev, V. M. Shulga, and V. I. Shnyrkov, Cryogenics **60**, 76 (2014).
[36]A. M. Korolev, V. M. Shulga, O. G. Turutanov, and V. I. Shnyrkov, Pribory i Tekhnika Eksperimenta **4**, 37 (2015) [Instrum. Exp. Techn. **58**, 478 (2015)].
[37]V. I. Shnyrkov and G. M. Tsoi, "Signal and noise characteristics of RF SQUIDs," in *Principles and Applications of Superconducting Quantum Interference Devices*, edited by A. Barone (World Scientific, Singapure, 1992), pp. 77–149.
[38]H. Ahola, G. J. Ehnholm, P. Ostman, and B. Rantala, J. Low Temp. Phys. **35**, 313 (1979).
[39]V. I. Shnyrkov, G. M. Tsoi, V. V. Kartsovnik, and S. S. Tinchev, Zh. Tekhn. Fiz. **53**, 1809 (1983).
[40]S. K. Tolpygo, V. Bolkhovsky, D. E. Oates, R. Rastogi, S. Zarr, A. L. Day, T. J. Weir, A. Wynn, and L. M. Johnson, IEEE Trans. Appl. Supercond. **28**, 1 (2018).
[41]M. Belogolovskii, E. Zhitlukhina, V. Lacquaniti, N. De Leo, M. Fretto, and A. Sosso, Fiz. Nizk. Temp. **43**, 950 (2017) [Low Temp. Phys. **43**, 756 (2017)].

Translated by AIP Author Services